

# Lawrence Berkeley National Laboratory

## LBL Publications

### Title

Absolute single photoionization cross-sections of Br<sup>3+</sup>: experiment and theory

### Permalink

<https://escholarship.org/uc/item/96v927tv>

### Journal

Journal of Physics B Atomic Molecular and Optical Physics, 52(14)

### ISSN

0953-4075

### Authors

Macaluso, DA

Aguilar, A

Kilcoyne, ALD

et al.

### Publication Date

2019-07-28

### DOI

10.1088/1361-6455/ab0e22

Peer reviewed

# Absolute single photoionization cross-sections of $\text{Br}^{3+}$ : Experiment and theory

D. A. Macaluso\*

*Department of Physics and Astronomy, University of Montana, Missoula, MT 59812*

A. Aguilar<sup>†</sup> and A. L. D. Kilcoyne

*The Advanced Light Source, Lawrence Berkeley National Laboratory, Berkeley, CA 94720*

R. C. Bilodeau

*Department of Physics, University of Connecticut, Storrs, CT 06269 and  
The Advanced Light Source, Lawrence Berkeley National Laboratory, Berkeley, CA 94720*

A. M. Juárez

*Instituto de Ciencias Físicas, Universidad Nacional Autónoma de México,  
PO Box 48-3, Cuernavaca 62251, Mor. México*

I. Dumitriu

*Department of Physics, Hobart and William Smith Colleges, Geneva, NY 14456*

D. Hardy<sup>‡</sup>

*Department of Physics and Astronomy, Louisiana State University, Baton Rouge, LA 70803 and  
The Advanced Light Source, Lawrence Berkeley National Laboratory, Berkeley, CA 94720*

N. C. Sterling

*Department of Physics, University of West Georgia, Carrollton, GA 30118*

M. Bautista

*Department of Physics, Western Michigan University, Kalamazoo, MI 49008-5252*

(Dated: November 7, 2018)

Absolute single photoionization cross section measurements for  $\text{Br}^{3+}$  ions were performed at the Advanced Light Source at Lawrence Berkeley National Laboratory using the merged-beams technique. Measurements were made at a photon energy resolution of  $21 \pm 3$  meV in the photon energy range 44.79 – 59.54 eV, spanning the ground state and low-lying metastable state ionization thresholds. Numerous resonance features in the experimental spectrum are assigned and their energies and quantum defect values are tabulated. The cross-section measurements are also compared with Breit-Pauli R-matrix calculations with suitable agreement over the photon energy range investigated. Analysis of the measured spectrum including Rydberg resonance series identifications produced a new **empirical** determination of the ionizational potential of  $\text{Br}^{3+}$  of  $46.977 \pm 0.050$  eV, which is 805 meV lower than the most recently published value of 47.782 eV. This disparity between our determination and the earlier published value is similar to an 843 meV shift in the accepted ionization potential published for iso-electronic  $\text{Se}^{2+}$  as part of this same research program.

PACS numbers: 32.80.Fb, 32.80.Aa, 32.70.Cs, 95.30.Dr

## I. INTRODUCTION

Bromine is one of several trans-iron elements (also known as neutron( $n$ )-capture elements) that have recently been detected in astronomical objects including stars [1, 2] and ionized nebulae [3, 4]. The abundances of  $n$ -capture elements in these objects provide unique insight into stellar nucleosynthesis and the chemical evolution of galaxies. Bromine has received recent interest

as observations have revealed spectroscopic features of its ions in chemically peculiar stars [5] and white dwarfs [6]. These objects exhibit Br abundances more than 100 times larger than in the Sun, likely due to chemical stratification by diffusion and radiative levitation processes. Moreover, a near-infrared transition of  $\text{Br}^{4+}$  was detected for the first time this year in planetary nebulae [7].

However, accurate abundance determinations strongly depend on the availability of accurate atomic data for processes governing its ionization equilibrium – data that is largely unknown for most  $n$ -capture element ions including those of Br. This problem is cast into relief by the fact that atomic data uncertainties alone can result in abundance errors in astrophysical nebulae of a factor of two or more [8, 9].

---

\* david.macaluso@umontana.edu

<sup>†</sup> Present address: ReVera Incorporated, 3090 Oakmead Village Drive, Santa Clara, CA 95051

<sup>‡</sup> Present address: Northrop Grumman, Elkton, MD 21921

To address this need, the present program was instituted to measure high-energy-resolution absolute photoionization cross sections for several of the  $n$ -capture elemental ions recently detected. The initial measurements of this program [10–16] have provided critically needed benchmarks to observational astronomers [9, 17, 18] that have been used to analyze astronomical spectra [19], contributed to the ongoing development of theoretical atomic physics codes [20–24], and updated tabulated thresholds and excited-state energy levels published in the NIST atomic spectra database [12, 13, 25].

In this report we present absolute single photoionization cross-section measurements of  $\text{Br}^{3+}$ . These measurements were performed using merged-beam photo-ion spectroscopy at a photon energy resolution of  $21 \pm 3$  meV in the photon energy range 44.79 to 59.54 eV. This energy range encompasses the ionization thresholds of the  $^3P_0$  ground state and three lowest energy excited states, the  $^3P_1$ ,  $^3P_2$ , and  $^1D_2$  states of  $\text{Br}^{3+}$ . Analysis of the resonance structure produced three distinct Rydberg resonance series identifications with one of the three series originating from multiple initial states of  $\text{Br}^{3+}$ . The remaining two series exhibit splitting due to variations in coupling between the excited electron and the ion core. This Rydberg series analysis was instrumental in determining the ground state ionization potential of  $\text{Br}^{3+}$  to be  $46.977 \pm 0.050$  eV which is 805 meV lower than the most recent published value for this system [25, 26].

## II. EXPERIMENT

The measurements were conducted at the Advanced Light Source (ALS) synchrotron radiation facility at Lawrence Berkeley National Laboratory using the ion-photon-beam (IPB) end station installed at undulator Beamline 10.0.1.2 [11–13, 27–35]. In the technique of merged-beams photo-ion spectroscopy, a beam of ions known as the *primary beam* is merged with an intense, counter-propagating beam of photons produced by a synchrotron light source. During this interaction, ions in the primary beam are further ionized when they eject one or more electrons via photon absorption. The resulting photo-ions constitute the *product beam* and are collected and counted as the photon energy is varied. By counting the number of product photo-ions produced as a function of photon energy, the photoionization spectra that are so critical to the analysis and interpretation of astronomical data are produced.

The details of merged-beams science are readily available in the literature ([36] and [37] for a broad overview), so the reader is encouraged to review the references for additional information that is beyond the scope of this report. For the purposes of this manuscript, the particular experimental details unique to this ion species are detailed below.

To produce the primary ion beam, tetrabromomethane (also known as carbon tetrabromide) vapor was intro-

duced into a 10 GHz electron-cyclotron-resonance (ECR) ion source [38, 39] via a precision leak valve. The resulting ions were accelerated out of the ion source via a 6 kV extraction potential. A  $60^\circ$  dipole analyzing magnet was used to select the  $\text{Br}^{3+}$  ion from the heterogeneous mixture of ion species present in the ECR ion source discharge. This is accomplished by exploiting the unique mass-to-charge ratio of the various  $\text{Br}^{n+}$  ions present in the source discharge. In doing so only the ion under investigation was allowed to pass unimpeded through the magnet apertures thus forming the homogeneous primary ion beam with primary beam currents typically in the 80 nA range for  $^{79}\text{Br}^{3+}$  and 120 nA range for  $^{80}\text{Br}^{3+}$  as measured on the primary beam Faraday cup. Measurements were made on both primary natural isotopes of Br depending on which provided a more stable primary ion beam under the particular experimental conditions at the time.

For relative spectroscopic measurements, photo-ions produced along the entire  $\sim 1.4$  m merged-beam path length were selected by the demerging magnet and directed into the detector assembly to be counted as a function of photon energy. The photon energy was varied in steps of  $\Delta E = 5$  meV for all spectroscopic measurements. Absolute photoionization cross sections were then measured at nine discrete energies that were chosen to get a broad sample of direct and resonant features spanning the majority of the spectroscopic energy range. These absolute cross-section measurements were then used during data analysis to place the relative spectroscopic measurements on an absolute scale (Figure 1). For the absolute cross-section measurements a potential of either +1.0 or +2.0 kV was applied to an electrically-isolated stainless-steel mesh cylinder  $29.4 \pm 0.56$  cm long. This cylinder is known as the *interaction region* and is coaxial with the photon and ion beams in the approximate center of the region of ion and photon beam overlap. The applied potential energy-tags the photo-ions produced within the interaction region's volume so that the demerging magnet can be tuned such that only those photo-ions are directed to the detector. This is done to isolate the photo-ions produced inside the cylinder, where beam overlaps are carefully monitored, from those produced outside the cylinder where there is no beam overlap monitoring. The overlap of the ion and photon beams within the interaction region was measured immediately before and after each absolute cross-section measurement using three translating slit scanners to accurately quantify their mutual volume of interaction. This volume, in combination with the primary ion and photon beam intensities, is used to calculate the absolute photoionization cross section values at each discrete energy. Uncertainties in the absolute measurements are calculated as a quadrature sum of the individual uncertainties that arise from the characterization of the ion and photon beams and their spatial overlap, and the physical and statistical collection of photo-ions. This total uncertainty is typically 15 - 17% and is thus conservatively estimated to be 20%

in the present analysis [28].

Photons were produced by electrons accelerated within a 10-cm period, 43 period undulator housed within the 1.9 GeV, 400 mA (at the time) constant-current storage ring of the ALS. Downstream of the undulator, a spherical-grating monochromator with three interchangeable diffraction gratings was used to select the particular photon energy and energy resolution of the collimated photon beam. The photon flux was monitored with a silicon photodiode (IRD, SXUV-100) referenced to a second photodiode from the same manufacturing batch that was absolutely calibrated by both NIST and the PTB at BESSY II in different photon energy ranges.

The contribution to the total photoionization cross section due to the production and transmission of higher-order radiation from the undulator and monochromator at Beamline 10 must be addressed [40]. A recently published analysis of the higher-order radiation content at Beamline 10 [12] found that second-order radiation is primarily off-axis and is mitigated by the use of lateral baffles on Beamline 10. The report also found that third-order photons represent a significant fraction of the photon beam only at the lowest energies of the low-energy grating (i.e., below 20 eV). By 30 eV, third-order photons were shown to represent less than 5 percent of the photon beam and by 40 eV this percentage is below 1 percent. This indicates the contribution to the measured photon flux from higher-order photons is insignificant in the energy range of these measurements and can be neglected in the calculation of absolute photoionization cross sections. To verify this, spectroscopic measurements were made at two-times and three-times the energy range of the observed spectrum, and no features similar to those measured in first order were found; thus second- and/or third-order photons were not responsible for the measured structure of the present experimental spectrum.

The photon energy scale for these measurements was calibrated using well-known autoionizing states of Kr [41, 42] and He [43] in first, second, and third order on a side-branch gas cell. These calibrations produced an energy uncertainty conservatively estimated to be  $\pm 50$  meV. The spectra were measured on multiple beamtimes over several years with energy calibrations that agree within the quoted energy uncertainty.

### III. RESULTS AND ANALYSIS

The  $\text{Br}^{3+}$  absolute single photoionization cross section spectrum is shown in Figure 1. The circles with error bars in the figure correspond to the nine absolute cross-section measurements (Table I) that were used to place the relative photo-ion yield spectrum on an absolute scale.

To identify and tabulate individual resonances as members of a given Rydberg resonance series, all significant resonance features are numbered as shown in Figure 2. The NIST Atomic Spectra Database [25] was the primary source for the  $\text{Br}^{3+}$  (Table II) and  $\text{Br}^{4+}$  (Table III)

TABLE I.  $\text{Br}^{3+}$  absolute single photoionization cross-sections measured at  $21 \pm 3$  meV photon energy resolution.

Energy (eV)	$\sigma$ (Mb)
44.800	$0.04 \pm 0.01$
46.000	$0.13 \pm 0.03$
47.700	$0.36 \pm 0.07$
48.442	$2.01 \pm 0.40$
49.956	$0.46 \pm 0.09$
52.656	$3.10 \pm 0.62$
53.400	$0.39 \pm 0.08$
54.573	$3.07 \pm 0.61$
55.200	$0.46 \pm 0.09$

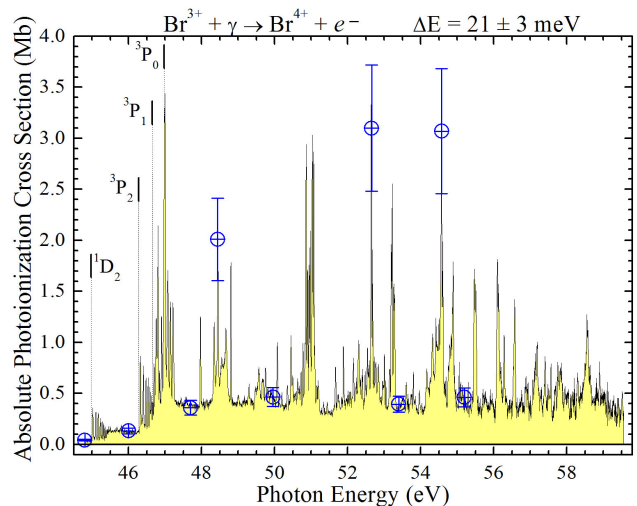


FIG. 1. (Color online) Absolute  $\text{Br}^{3+} \rightarrow \text{Br}^{4+}$  photoionization cross section measured at  $21 \pm 3$  meV photon energy resolution. Circles with error bars represent absolute cross-section measurements used to place the relative photo-ion yield spectrum on an absolute scale (Table I). The  $^3P_0$  ground state and  $^3P_1$ ,  $^3P_2$ , and  $^1D_2$  metastable state ionization thresholds from NIST [25] are indicated by vertical bars with dashed lines.

energy levels used in the Rydberg series analysis. The Cowan atomic structure code available online from Los Alamos National Laboratory [44] was also used during this stage of analysis. While the Cowan code typically cannot be used to reliably determine absolute energies, it is an efficient method for calculating approximate energy differences between initial and intermediate Rydberg states or for level splittings between common  $J$ -term states, for example. In the present analysis the Cowan code was used to calculate the approximate excited-state energy levels of the  $^4P_{1/2}$ ,  $^4P_{3/2}$  and  $^4P_{5/2}$  states of  $\text{Br}^{3+}$  as these states are known to exist but have not been measured and thus do not appear in the NIST database (Table III).

Rydberg series analysis was based on the quantum de-

TABLE II. Energy levels of  $\text{Br}^{3+}$  tabulated by NIST [25] and determined in the present analysis. Quoted uncertainties in the excited state energy levels are relative to the experimentally determined ground state ionization potential.

Configuration	Term	$J$	NIST (eV)	Experiment (eV)
$3d^{10}4s^24p^2$	$^3P$	0	0.000	$0.000 \pm 0.000$
		1	0.325	$0.325 \pm 0.005$
		2	0.696	$0.696 \pm 0.005$
	$^1D$	2	2.007	$2.007 \pm 0.005$

TABLE III. Energy levels of  $\text{Br}^{4+}$  tabulated by NIST [25] and determined in the present analysis. Quoted uncertainties in the excited state energy levels are relative to the experimentally determined ground state ionization potential.

Configuration	Term	$J$	NIST (eV)	Exp. (eV)
$3d^{10}4s^24p$	$^2P^o$	1/2	0.000	$0.000 \pm 0.000$
		3/2	0.755	$0.770 \pm 0.005$
$3d^{10}4s4p^2$	$^4P$	1/2	11.597 <sup>a</sup>	NA
		3/2	11.903 <sup>a</sup>	$11.953 \pm 0.005$
		5/2	12.313 <sup>a</sup>	NA
	$^2D$	5/2	15.328	$15.345 \pm 0.005$

<sup>a</sup> These values do not appear in the NIST database and were instead taken from [45].

fect form of the Rydberg formula [46],

$$E_n = E_\infty - \frac{(Z - N_c)^2}{(n - \delta_n)^2} \quad (1)$$

where  $E_n$  is the energy of the  $n$ th resonance,  $E_\infty$  is the series limit corresponding to the direct ionization energy of the excited Rydberg electron (where  $n = \infty$ ),  $Z$  is the charge of the primary ion nucleus,  $N_c$  is the number of core electrons,  $n$  is the principal quantum number of the identified resonance, and  $\delta$  is the quantum defect parameter. The  $\delta$  parameter quantifies the deviation from a purely hydrogenic model due to incomplete screening of the nucleus as a result of core penetration by the excited electron. Quantum defect values are usually between 0 and 1 where negative values or values greater than 1 typically indicate an incorrect principal quantum number assignment for a particular resonance or resonance series. Quantum defect values were free parameters in the present analysis; however, they were constrained to remain between 0 and 1 and be constant for a given series identification.

As seen in the Rydberg formula,  $\delta$  values are a function of  $n$  and the excitation energy of each resonance for a given series assignment, so the uncertainty in  $\delta$  is related to the energy uncertainty and resolution of these

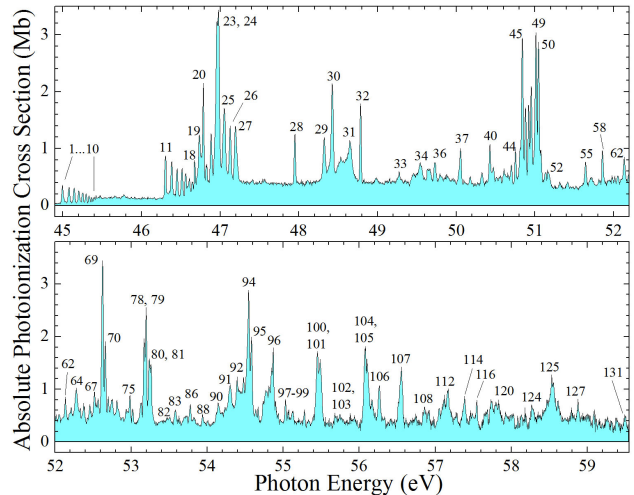


FIG. 2. (Color online) Resonance feature numbering scheme used in the  $\text{Br}^{3+}$  Rydberg series identification tables.

measurements. In cases where multiple peaks coincide, the ability to distinguish individual resonances also affects the determination of  $\delta$  values. In addition, the  $\delta$  parameter has decreasing influence on the calculated resonance energy as the quantum number increases so each  $\delta$  has its own unique uncertainty. Due to the complexity of these relations, error bars for  $\delta$  have been omitted and the presented  $\delta$  values can be considered accurate to within the quoted energy uncertainty and resolution of these measurements.

For Rydberg series analysis, the ionization potential of  $\text{Br}^{3+}$ , excited state energies of  $\text{Br}^{3+}$  and  $\text{Br}^{4+}$ , and subsequent series limits were initially set using NIST-reported values. However, initial identifications were impossible as the reported ionization potential for  $\text{Br}^{3+}$  of 47.782 eV was in clear disagreement with the measured spectrum as indicated in Figure 3. The reported thresholds for the low-lying  $^1D_2$  and  $^3P_2$  metastable states, whose locations are a function of the reported ground state ionization potential (IP), were shifted well above the observed onset of their corresponding Rydberg series. This shift is shown in the figure with arrows indicating where the thresholds *should* be to match the features of the experimental spectrum. No other levels exist to which these Rydberg series can be attributed so this discrepancy forced the IP to be decreased significantly to align the measured resonances with their corresponding thresholds. The measured spectrum imposes an additional constraint on the locations of these thresholds; they cannot be lower than the predicted energy location of the next lower-energy resonance in each series. That is, these series both begin with an  $n=18$  resonance so the  $n=17$  resonance is not seen in the photo-ion spectrum and it therefore must lie below threshold. Thus the measured spectrum constrains the thresholds for these states to exist within a narrow window bounded on the high-energy side by the first ob-

served resonance of the series and on the low-energy side by the predicted location of the next lower resonance. Once the ground state ionization potential was shifted such that the metastable state thresholds both fell within these windows, the Rydberg series identifications were then used to fine tune the IP to get the most consistent agreement between published excited-state energy level values and the identifications. This ultimately produced a decrease in the ground state ionization potential of 805 meV to the presently determined value of 46.997 eV.

A shift of similar magnitude was found by this same program in the isoelectronic ion  $\text{Se}^{2+}$  [14]. In that project a shift of 867 meV was required to align these same series. Our newly determined value for the ionization potential of  $\text{Se}^{2+}$  was independently corroborated by the authors of the original published IP (Tauheed *et al* of Aligarh Muslim University, who also provided the IP for  $\text{Br}^{3+}$ ) who had updated their determination of the IP of  $\text{Se}^{2+}$  to a value that agreed with this program's findings to within the combined uncertainties of the two experiments [14, 47]. As an additional indication of the reliability of these updated IP values, the Rydberg series identifications could not proceed in either system unless the published energy levels of the excited states of  $\text{Se}^{2+}$ ,  $\text{Se}^{3+}$ ,  $\text{Br}^{3+}$ , and  $\text{Br}^{4+}$  explored in this and the previous analysis were significantly altered. In other words, for this to be a systematic error in our energy scale calibration it would require multiple accepted levels in four ions to be inaccurate. It would also indicate our energy scale calibration is shifted by a factor 16-times greater than the conservatively estimated energy uncertainty of ALS Beamline 10.0.1.2. In both the previous Se project and the present analysis, the corresponding Rydberg series identifications progressed smoothly once the ionization potential was adjusted to match the experimental data.

Three distinct Rydberg resonance series have been identified in the experimental spectrum (Figure 4). These series arise from the  $^3P_1$ ,  $^3P_2$ , and  $^1D_2$  metastable states of  $\text{Br}^{3+}$  and are due to  $4s \rightarrow np$  and  $4p \rightarrow nd$  autoionizing transitions. The first identified series is the series originating from the  $^3P_1$ ,  $^3P_2$ , and  $^1D_2$  states that was instrumental in determining the updated ionization potential. The limit of this closely spaced series is the  $^2P_{3/2}$  excited state of  $\text{Br}^{4+}$  and is seen in Figure 4 originating from the  $^1D_2$  state (green solid triangles), the  $^3P_2$  state (violet bottom-half-filled triangles), and the  $^3P_1$  state (pink top-half-filled triangles). The initial resonances of each of these three instances of this series are  $n_o = 18$ , where  $n_o$  is the principal quantum number of the first intermediate energy level to which the Rydberg electron is excited before relaxing via autoionization with emission of an Auger electron. Owing to the significance of this series in the present analysis, these identifications are isolated and expanded in Figure 5 with the details of this series presented in Table IV. Note that the resonance energies listed in the Rydberg series tables are *predicted* energies using the quantum defect form of the Rydberg formula. The associated resonance identifications seen in

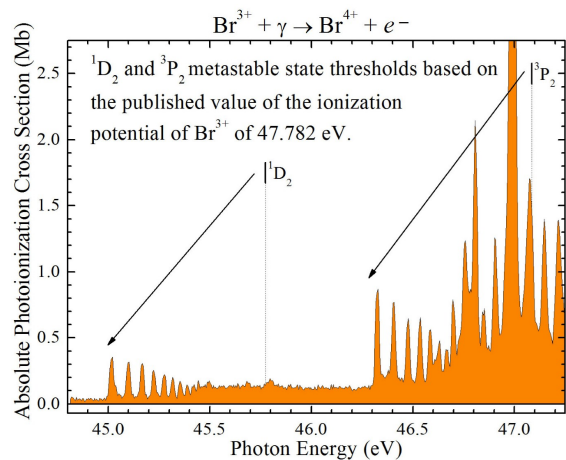


FIG. 3. (Color online) The reported ionization thresholds for the  $^3P_2$  and  $^1D_2$  metastable states are indicated by vertical bars with dashed droplines [25]. These thresholds are in clear disagreement with the onset of their associated Rydberg series. The arrows indicate the approximate locations where these thresholds *should* be in the measured spectrum.

Figures 4 and 5 are these predicted energies plotted on the measured spectrum with the correspondence between calculated and measured resonance energies highlighted via dashed droplines.

A second Rydberg series is seen originating from the  $^3P_1$  initial state of  $\text{Br}^{3+}$  with a series limit in the  $^4P_{3/2}$  excited state of  $\text{Br}^{4+}$ . This final state is at a significantly higher energy than the previous  $^2P_{3/2}$  series limit and thus this series spans a much wider energy range. The series is indicated in Figure 4 by blue right-half-filled triangles with dashed droplines with the first resonance of this series at  $n_o = 5$ . In this  $n_o = 5$  resonance, five distinct features are resolved and are seen tightly clustered around the  $^3P_0$  ground state ionization threshold. This cluster of resonances corresponds to level splitting of the intermediate Rydberg state. The coupling variations remain fully resolved for just this initial resonance and are seen overlapping and combining in subsequent resonances and become indistinguishable at  $n = 11$ . The  $^4P_{3/2}$  series limit final state for this series was determined using published energy-level values of  $\text{Br}^{4+}$  from A. Tauheed and Y. N. Joshi (2009 [45]). The details of this series are listed in Table V.

The final identified Rydberg series originates from the  $^1D_2$  state of  $\text{Br}^{3+}$  and converges to the  $^2D_{5/2}$  series limit in  $\text{Br}^{4+}$ . The series is indicated in Figure 4 by red left-half-filled triangles with dashed droplines with the first resonance of this series at  $n_o = 5$ . In this  $n_o = 5$  resonance, five distinct features are resolved as seen in the region immediately beyond the  $^3P_0$  ground state ionization threshold of Figure 4. This cluster of resonances corresponds to similar level splitting of the intermediate Rydberg state as seen in the previous series. The coupling variations remain fully resolved for just the initial



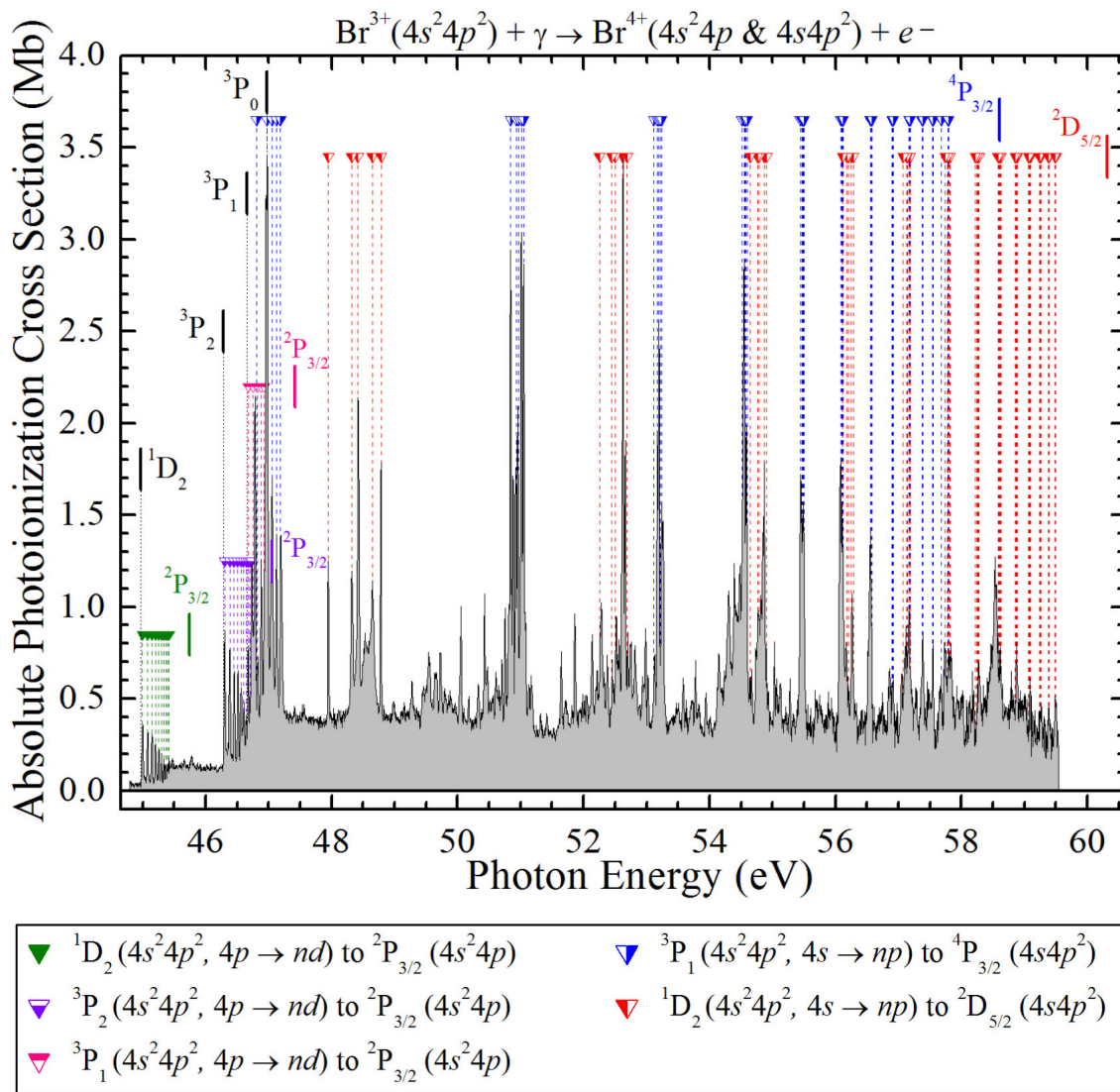


FIG. 4. (Color online) Rydberg series of resonances due to  $4s \rightarrow np$  transitions converging to the  $4s^24p$  ( $^2P_{3/2}$ ) and  $4s4p^2$  ( $^4P_{3/2}$ ,  $^2D_{5/2}$ ) series limits in  $\text{Br}^{4+}$ . The ionization thresholds for the  $^3P_0$  ground state and  $^3P_1$ ,  $^3P_2$ , and  $^1D_2$  metastable states are indicated by black vertical bars with dashed droplines. The series limits for each series where  $n = \infty$  are indicated by vertical bars without droplines; the series limits are at the same vertical location as their associated series symbols, are color coordinated, and are labeled with the corresponding final state of  $\text{Br}^{4+}$  for that series.

resonance once again and are seen overlapping and combining in subsequent resonances and become unresolved by  $n = 11$  as well. The details of this series are listed in Table VI.

#### IV. THEORY

We used the R-matrix method to compute the photoionization cross sections of  $\text{Br}^{3+}$ . To this end, we represented the  $\text{Br}^{3+}$  target ion by a CI expansion of the configurations  $4s^24p^2$ ,  $4s4p^3$ ,  $4s^24p4d$ ,  $4s^24p5s$ ,  $4s4p^24d$ ,  $4s4p^25s$ ,  $4s4p^25p$ ,  $4p^4$ ,  $4s^24d^2$ ,  $4s^25s^2$ ,  $4s^25p^2$ ,  $4p^34d$ ,  $4p^35s$ , and  $4p^35p$ .

We used the Thomas-Fermi-Dirac-Amaldi potential in the code AUTOSTRUCTURE [46, 48] to compute orthogonal radial wave functions for all orbitals. The scaling factors for each orbital are optimized in a multiconfiguration variational procedure minimizing a weighted average of LS term energies that account for one-body Breit-Pauli (BP) effects.

For the scattering calculation, we employ the Breit-Pauli R-matrix set of codes [49, 50] to compute the photoionization cross sections for the  $4s^24p^2$ ,  $^3P$  and  $^1D$  LS terms. Our close coupling expansion includes the lowest fifteen multiplets of the target ions. The cross sections were sampled at evenly spaced photon energy intervals of 0.0245 eV. The cross sections of the three

TABLE IV. Rydberg series of resonances due to  $4p \rightarrow nd$  transitions from the  $^1D_2$ ,  $^3P_2$ , and  $^3P_1$  excited states of  $\text{Br}^{3+}$  converging to the  $^2P_{3/2}$  series limit in  $\text{Br}^{4+}$  (green solid triangles for the series originating from the  $^1D_2$  state, violet bottom-half-filled triangles from the  $^3P_2$  state, and pink top-half-filled triangles from the  $^3P_1$  state as seen in Figures 4 and 5). Tabulated feature numbers correspond to those identified in Figure 2.

Initial $\text{Br}^{3+}$ States: $^1D_2, ^3P_2, ^3P_1, 4s^24p^2$ Final $\text{Br}^{4+}$ State: $^2P_{3/2}, 4s^24p$											
Rydberg Series $4s^24p^2 (^1D_2), 4p \rightarrow nd$				Rydberg Series $4s^24p^2 (^3P_2), 4p \rightarrow nd$				Rydberg Series $4s^24p^2 (^3P_1), 4p \rightarrow nd$			
$n$	Energy (eV)	$\delta$	Feature #	$n$	Energy (eV)	$\delta$	Feature #	$n$	Energy (eV)	$\delta$	Feature #
18	44.995	0.902	31	18	46.303	0.948	25	18	46.675	0.928	1
19	45.075	0.902	34	19	46.383	0.948	26	19	46.755	0.928	2
20	45.143	0.902	38	20	46.451	0.948	27	20	46.823	0.928	3
21	45.201	0.902	42	21	46.510	0.948	28	21	46.882	0.928	4
22	45.251	0.902	47	22	46.560	0.948	29	22	46.932	0.928	5
23	45.294	0.902	49	23	46.604	0.948	30				
24	45.332	0.902	50	24	46.642	0.948	31				
25	45.365	0.902	51	25	46.675	0.948	32				
26	45.394	0.902	52	26	46.704	0.948	33				
27	45.420	0.902	53	27	46.730	0.948	34				
$\infty$	<b>45.740</b>			$\infty$	<b>47.051</b>			$\infty$	<b>47.422</b>		

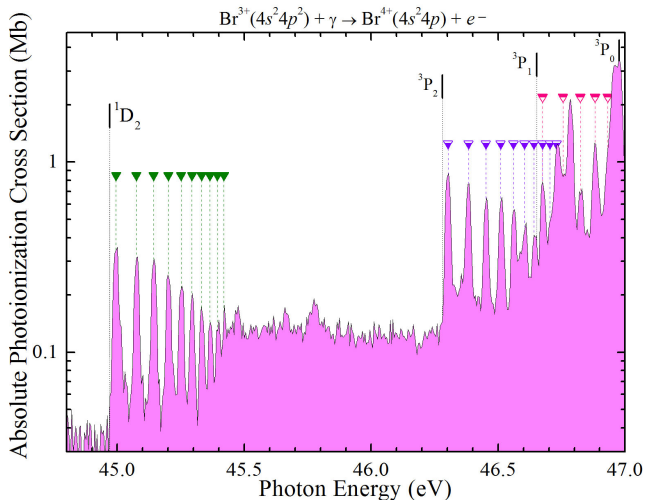


FIG. 5. (Color online) Rydberg series of resonances due to  $4s \rightarrow np$  transitions converging to the  $4s^24p (^2P_{3/2})$  series limit in  $\text{Br}^{4+}$  (green solid triangles for the series originating from the  $^1D_2$  state, violet bottom-half-filled triangles from the  $^3P_2$  state, and pink top-half-filled triangles from the  $^3P_1$  state). The ionization thresholds for the  $^3P_0$  ground state and  $^3P_1$ ,  $^3P_2$ , and  $^1D_2$  metastable states are indicated by vertical bars with dashed droplines [25]. The spectrum has been placed on a semi-logarithmic scale to compress the vertical scale and emphasize the two lowest-lying metastable state Rydberg series as these well-defined series were critical in the determination of the ionization potential of  $\text{Br}^{3+}$ .

states were then weighted by their statistical multiplicities and added. The resulting theoretical spectrum was aligned with the onsets of the measured metastable state

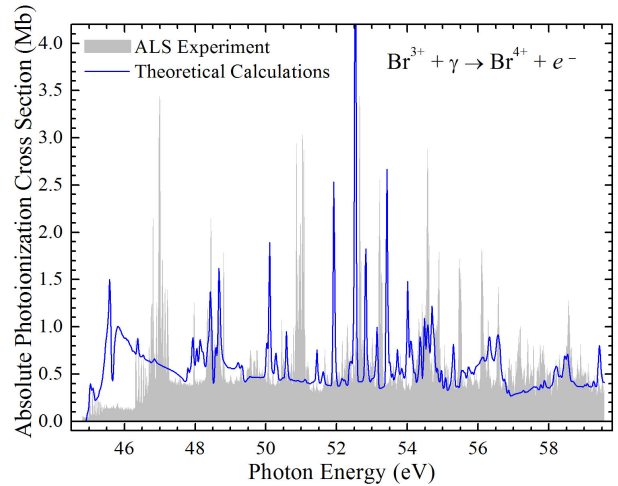


FIG. 6. (Color online) Comparison of the  $21 \pm 3$  meV energy-resolution experimental spectrum (gray fill) with the Breit-Pauli R-matrix calculations (blue line).

thresholds as seen in Figure 6. While the locations and relative intensities of the resonant features in the theoretical spectrum generally agree favorably with experiment, significant features present in the experimental cross section are predicted at different energy locations and different strengths by theoretical calculations. This highlights the challenges faced by theoretical methods in reproducing accurate positions for highly mixed autoionizing states, particularly in heavy ionic systems that likely are susceptible to orbital relaxation effects. This also supports the need for accurate, high-resolution absolute cross section measurements such as these to inform



TABLE V. Rydberg series of resonances due to  $4s \rightarrow np$  transitions from the  $^3P_1$  state of  $\text{Br}^{3+}$  converging to the  $^4P_{3/2}$  series limit in  $\text{Br}^{4+}$  (blue right-half-filled triangles in Figure 4). Five unique instances of this series were observed as differentiated by variations in intermediate excited-state coupling with the first 4-5 resonances resolved. Tabulated feature numbers correspond to those identified in Figure 2.

<b>Initial <math>\text{Br}^{3+}</math> State: <math>^3P_1, 4s^24p^2</math></b> <b>Final <math>\text{Br}^{4+}</math> State: <math>^4P_{3/2}, 4s4p^2</math></b>											
Rydberg Series $4s^24p^2(^3P_1), 4s \rightarrow np$				Rydberg Series $4s^24p^2(^3P_1), 4s \rightarrow np$				Rydberg Series $4s^24p^2(^3P_1), 4s \rightarrow np$			
$n$	Energy (eV)	$\delta$	Feature #	$n$	Energy (eV)	$\delta$	Feature #	$n$	Energy (eV)	$\delta$	Feature #
5	46.808	0.704	20	5	46.969	0.675	24	5	47.050	0.656	25
6	50.843	0.704	45	6	50.929	0.675	47	6	50.972	0.656	48
7	53.113	0.704	77	7	53.164	0.675	78	7	53.190	0.656	79
8	54.515	0.704	94	8	54.548	0.675	94	8	54.565	0.656	94
9	55.442	0.704	100	9	55.464	0.675	100/101	9	55.476	0.656	100/101
10	56.086	0.704	104	10	56.102	0.675	105	10	56.110	0.656	105
11	56.551	0.704	107	11	56.563	0.675	107	11	56.569	0.656	107
12	56.899	0.704	109	12	56.908	0.675	109	12	56.912	0.656	109
13	57.165	0.704	112	13	57.172	0.675	112	13	57.175	0.656	112
14	57.374	0.704	114	14	57.379	0.675	114	14	57.382	0.656	114
15	57.540	0.704	116	15	57.544	0.675	116	15	57.546	0.656	116
16	57.674	0.704	117	16	57.678	0.675	117	16	57.680	0.656	117
17	57.785	0.704	119	17	57.788	0.675	119	17	57.790	0.656	119
$\infty$	<b>58.605</b>			$\infty$	<b>58.605</b>			$\infty$	<b>58.605</b>		

Rydberg Series $4s^24p^2(^3P_1), 4s \rightarrow np$				Rydberg Series $4s^24p^2(^3P_1), 4s \rightarrow np$			
$n$	Energy (eV)	$\delta$	Feature #	$n$	Energy (eV)	$\delta$	Feature #
5	47.125	0.645	26	5	47.190	0.633	27
6	51.013	0.645	48	6	51.047	0.633	50
7	53.214	0.645	79/80	7	53.235	0.633	80
8	54.580	0.645	95	8	54.594	0.633	95
9	55.486	0.645	101	9	55.495	0.633	101
10	56.117	0.645	105	10	56.124	0.633	105
11	56.575	0.645	107	11	56.579	0.633	107
12	56.916	0.645	109	12	56.920	0.633	109
13	57.179	0.645	112	13	57.182	0.633	112
14	57.384	0.645	114	14	57.387	0.633	114
15	57.548	0.645	116	15	57.550	0.633	116
16	57.682	0.645	117	16	57.683	0.633	117
17	57.791	0.645	119	17	57.792	0.633	119
$\infty$	<b>58.605</b>			$\infty$	<b>58.605</b>		

and guide the ongoing development of theoretical calculation codes while simultaneously providing astronomers and other end users with data that is otherwise not available by current theoretical methods.

## V. SUMMARY

We have presented absolute single photoionization cross-section measurements for  $\text{Br}^{3+}$  from the metastable state ionization region to above the ground state ionization threshold at a photon energy resolution of  $21 \pm 3$  meV. Initial analysis indicated a discrepancy between the reported and measured ionization potentials which necessitated a decrease in the reported ionization poten-

tial of  $\text{Br}^{3+}$  of 0.805 eV to the newly determined value of  $46.977 \pm 0.050$  eV. A similar shift was discovered in isoelectronic  $\text{Se}^{2+}$  by this same research program thus the newly established ionization potential of  $\text{Br}^{3+}$  is in excellent agreement with a previously published improvement on a similar system.

Three distinct Rydberg resonance series have been identified in the spectra of  $\text{Br}^{3+}$ . One series of the form  $4s \rightarrow np$  is identified originating from the  $^1D_2$  metastable state of  $\text{Br}^{3+}$  and converging to the  $^2D_{5/2}$  series limit in  $\text{Br}^{4+}$ . A second  $4s \rightarrow np$  series is identified originating from the  $^3P_1$  metastable state of  $\text{Br}^{3+}$  and converging to the  $^4P_{3/2}$  series limit in  $\text{Br}^{4+}$ . Five separate instances of each of these series were observed to arise from coupling variations between the core and the ex-

TABLE VI. Rydberg series of resonances due to  $4s \rightarrow np$  transitions from the  $^1D_2$  state of  $\text{Br}^{3+}$  converging to the  $^2D_{5/2}$  series limit in  $\text{Br}^{4+}$  (red left-half-filled triangles in Figure 4). Five unique instances of this series were observed as differentiated by variations in intermediate excited-state coupling with only the first 2 resonances fully resolved. Tabulated feature numbers correspond to those identified in Figure 2.

<b>Initial <math>\text{Br}^{3+}</math> state: <math>^1D_2, 4s^24p^2</math></b> <b>Final <math>\text{Br}^{4+}</math> state: <math>^2D_{5/2}, 4s4p^2</math></b>											
Rydberg Series $4s^24p^2(^1D_2), 4s \rightarrow np$				Rydberg Series $4s^24p^2(^1D_2), 4s \rightarrow np$				Rydberg Series $4s^24p^2(^1D_2), 4s \rightarrow np$			
$n$	Energy (eV)	$\delta$	Feature #	$n$	Energy (eV)	$\delta$	Feature #	$n$	Energy (eV)	$\delta$	Feature #
5	47.950	0.804	28	5	48.320	0.740	29	5	48.419	0.722	30
6	52.251	0.804	64	6	52.447	0.740	66	6	52.500	0.722	67
7	54.644	0.804	96	7	54.760	0.740	96	7	54.791	0.722	96
8	56.111	0.804	104	8	56.185	0.740	105	8	56.205	0.722	105
9	57.074	0.804	110	9	57.124	0.740	111	9	57.138	0.722	111
10	57.740	0.804	118	10	57.776	0.740	119	10	57.786	0.722	119
11	58.221	0.804	123	11	58.247	0.740	123	11	58.254	0.722	123
12	58.578	0.804	125	12	58.598	0.740	126	12	58.603	0.722	126
13	58.851	0.804	127	13	58.866	0.740	127	13	58.871	0.722	127
14	59.065	0.804	128	14	59.077	0.740	128	14	59.080	0.722	128
15	59.234	0.804	129	15	59.244	0.740	129	15	59.247	0.722	129
16	59.372	0.804	130	16	59.380	0.740	130	16	59.382	0.722	130
17	59.485	0.804	131	17	59.491	0.740	131	17	59.493	0.722	131
$\infty$	<b>60.315</b>			$\infty$	<b>60.315</b>			$\infty$	<b>60.315</b>		
Rydberg Series $4s^24p^2(^1D_2), 4s \rightarrow np$				Rydberg Series $4s^24p^2(^1D_2), 4s \rightarrow np$							
$n$	Energy (eV)	$\delta$	Feature #	$n$	Energy (eV)	$\delta$	Feature #				
5	48.644	0.681	31	5	48.784	0.655	32				
6	52.620	0.681	69	6	52.695	0.655	71				
7	54.863	0.681	96	7	54.907	0.655	96				
8	56.251	0.681	106	8	56.280	0.655	106				
9	57.169	0.681	112	9	57.189	0.655	112				
10	57.808	0.681	119	10	57.822	0.655	120				
11	58.270	0.681	123	11	58.281	0.655	123				
12	58.616	0.681	126	12	58.623	0.655	126				
13	58.880	0.681	127	13	58.886	0.655	127				
14	59.087	0.681	128	14	59.092	0.655	128				
15	59.253	0.681	129	15	59.257	0.655	129				
16	59.387	0.681	130	16	59.390	0.655	130				
17	59.497	0.681	131	17	59.500	0.655	131				
$\infty$	<b>60.315</b>			$\infty$	<b>60.315</b>						


cited electron. Finally, a Rydberg series of the form  $4p \rightarrow nd$  and originating from the  $^3P_1$ ,  $^3P_2$  and  $^1D_2$  metastable states was found converging to the  $^2P_{3/2}$  series limit in  $\text{Br}^{4+}$ . This series was instrumental in determining the improved ionization potential of ground state  $\text{Br}^{3+}$ . Resonances energies and quantum defects for all three series have been tabulated in Tables IV, V, and VI for completeness. Theoretical calculations were performed using the Thomas-Fermi-Dirac-Amaldi potential in AUTOSTRUCTURE and employing the Breit-Pauli R-matrix set of codes which produced suitable agreement with the experimental spectrum.

## ACKNOWLEDGMENTS

We gratefully acknowledge support from the NSF through award AST-1412928. D Macaluso gratefully acknowledges support from the Montana Space Grant Consortium. R Bilodeau gratefully acknowledges support from the US Department of Energy, Office of Science, Basic Energy Sciences (BES), Division of Chemical Sciences, Geosciences, and Biosciences under grant No. DE-SC0012376. Data acquired at beamline 10.0.1.2 at the Advanced Light Source, which is supported by the Director, Office of Science, Office of Basic Energy Sciences, of the US Department of Energy under contract No. DE-AC02-05CH11231. This research also used resources of the Oak Ridge Leadership Computing Facility at the Oak

Ridge National Laboratory, which is supported by the Of-

fice of Science of the U.S. Department of Energy (DoE) under Contract No. DE-AC05-00OR22725.

- 
- [1]  J. Roederer, *Astrophys. J.* **756**, 36 (2012).
- [2] I. U. Roederer, J. J. Cowan, G. W. Preston, S. A. Shechtman, C. Sneden, and I. B. Thompson, *Mon. Not. Roy. Astron. Soc.* **445**, 2970 (2012).
- [3] N. C. Sterling and H. L. Dinerstein, *Astrophys. J. Suppl. Ser.* **174**, 158 (2008).
- [4] N. Sterling, H. Dinerstein, K. Kaplan, and M. Bautista, *Astrophys. J. Let.* **819**, L9 (2016).
- [5] C. Cowley and G. Wahlgren, *AA* **447**, 681 (2006).
- [6] K. Werner, T. Rauch, M. Knorzer, and J. Kruk, *AA* **614**, A96 (2018), arXiv:1803.04809 [astro-ph.SR].
- [7] S. Madonna, M. Bautista, H. Dinerstein, N. Sterling, J. Garcia-Rojas, K. Kaplan, M. del Mar Rubio-Diez, N. Castro-Rodriguez, and F. Garzon, *Apj.* **861**, L8 (2018), arXiv:1806.05458.
- [8] N. C. Sterling, H. L. Dinerstein, and T. R. Kallman, *Astrophys. J. Suppl. Ser.* **169**, 37 (2007).
- [9] N. C. Sterling, R. L. Porter, and H. L. Dinerstein, *Astrophys. J. Suppl. Ser.* **218**, 25 (2015).
- [10] N. C. Sterling, M. C. Witthoef, D. A. Esteves, R. C. Bilodeau, A. L. D. Kilcoyne, E. C. Red, R. A. Phaneuf, G. A. Alna'Washi, and A. Aguilar, *Can. J. Phys.* **89**, 379 (2011).
- [11] N. C. Sterling, D. A. Esteves, R. C. Bilodeau, A. L. D. Kilcoyne, E. C. Red, R. A. Phaneuf, and A. Aguilar, *J. Phys. B: At. Mol. Opt. Phys.* **44**, 025701 (2011).
- [12] D. A. Esteves, R. C. Bilodeau, N. C. Sterling, R. A. Phaneuf, A. L. D. Kilcoyne, E. C. Red, and A. Aguilar, *Phys. Rev. A* **84**, 013406 (2011).
- [13] D. A. Esteves, R. C. Bilodeau, R. A. Phaneuf, A. L. D. Kilcoyne, E. C. Red, and A. Aguilar, *J. Phys. B: At. Mol. Opt. Phys.* **45**, 115201 (2012).
- [14] D. A. Macaluso, A. Aguilar, A. L. D. Kilcoyne, E. C. Red, R. C. Bilodeau, R. A. Phaneuf, N. C. Sterling, and B. M. McLaughlin, *Phys. Rev. A* **92**, 063424 (2015).
- [15] D. A. Macaluso, K. Bogolub, A. Johnson, A. Aguilar, A. L. D. Kilcoyne, R. C. Bilodeau, M. Bautista, A. B. Kerlin, and N. C. Sterling, *J. Phys. B: At. Mol. Opt. Phys.* **49**, 235002 (2016).
- [16] D. A. Macaluso, K. Bogolub, A. Johnson, A. Aguilar, A. L. D. Kilcoyne, R. C. Bilodeau, M. Bautista, A. B. Kerlin, and N. C. Sterling, *Journal of Physics B: Atomic, Molecular and Optical Physics* **50**, 119501 (2017).
- [17] N. C. Sterling, *Astron. Astrophys.* **533**, A62 (2011).
- [18] N. C. Sterling and M. C. Witthoef, *Astron. Astrophys.* **529**, A147 (2011).
- [19] N. C. Sterling, S. Madonna, K. Butler, J. García-Rojas, A. L. Mashburn, C. Morisset, V. Luridiana, and I. U. Roederer, *Astrophys. J.* **840**, 80 (2017), arXiv:1704.00741 [astro-ph.SR].
- [20] P. G. Burke, *R-Matrix Theory of Atomic Collisions: Application to Atomic, Molecular and Optical Processes* (Springer, New York, USA, 2011).
- [21] DARC codes URL, <http://connorb.freeshell.org>.
- [22] V. Fivet, M. Bautista, and C. Ballance, *J. Phys. B: At. Mol. Opt. Phys.* **45**, 035201 (2012).
- [23] B. M. McLaughlin and C. P. Ballance, *J. Phys. B: At. Mol. Opt. Phys.* **45**, 095202 (2012).
- [24] B. M. McLaughlin and C. P. Ballance, *J. Phys. B: At. Mol. Opt. Phys.* **45**, 085701 (2012).
- [25] A. Kramida, Y. Ralchenko, J. Reader, and NIST ASD Team, NIST Atomic Spectra Database (ver. 5.5.6), [Online]. Available: <https://physics.nist.gov/asd> [2018, August 6]. National Institute of Standards and Technology, Gaithersburg, MD. (2018).
- [26] A. Riyaz, K. Rahimullah, and A. Tauheed, *J Quant Spectrosc Radiat Transf.* **133**, 624 (2014).
- [27] A. M. Covington, A. Aguilar, I. R. Covington, M. F. Gharaibeh, C. A. Shirley, R. A. Phaneuf, I. Álvarez, C. Cisneros, G. Hinojosa, J. D. Bozek, I. Dominguez, M. M. Sant'Anna, A. S. Schlachter, N. Berrah, S. N. Nahar, and B. M. McLaughlin, *Phys. Rev. Lett.* **87**, 243002 (2001).
- [28] A. M. Covington, A. Aguilar, I. R. Covington, M. F. Gharaibeh, G. Hinojosa, C. A. Shirley, R. A. Phaneuf, I. Álvarez, C. Cisneros, I. Dominguez-Lopez, M. M. Sant'Anna, A. S. Schlachter, B. M. McLaughlin, and A. Dalgarno, *Phys. Rev. A* **66**, 062710 (2002).
- [29] G. A. Alna'washi, M. Lu, M. Habibi, R. A. Phaneuf, A. L. D. Kilcoyne, A. S. Schlachter, C. Cisneros, and B. M. McLaughlin, *Phys. Rev. A* **81**, 053416 (2010).
- [30] M. Habibi, D. Esteves, R. A. Phaneuf, A. L. D. Kilcoyne, A. Aguilar, and C. Cisneros, *Phys. Rev. A* **80**, 033407 (2009).
- [31] M. Gharaibeh, A. Aguilar, A. M. Covington, E. D. Emons, S. W. J. Scully, R. A. Phaneuf, and A. Müller, *Phys. Rev. A* **83**, 043412 (2011).
- [32] A. M. Covington, A. Aguilar, I. R. Covington, G. Hinojosa, C. A. Shirley, R. A. Phaneuf, I. Álvarez, C. Cisneros, I. Dominguez-Lopez, M. M. Sant'Anna, A. S. Schlachter, C. P. Ballance, and B. M. McLaughlin, *Phys. Rev. A* **84**, 013413 (2011).
- [33] J. M. Bizau, C. Blancard, M. Coreno, D. Cubaynes, C. Dehon, N. E. Hassan, F. Folkmann, M. F. Gharaibeh, A. Giuliani, J. Lemaire, A. R. Milosavljevi, C. Nicolas, and R. Thissen, *J. Phys. B: At. Mol. Opt. Phys.* **44**, 055205 (2011).
- [34] A. Müller, S. Schippers, D. Esteves-Macaluso, M. Habibi, A. Aguilar, A. L. D. Kilcoyne, R. A. Phaneuf, C. P. Ballance, and B. M. McLaughlin, *J. Phys. B: At. Mol. Opt. Phys.* **47**, 215202 (2014).
- [35] E. M. Hernández, A. M. Juárez, A. L. D. Kilcoyne, A. Aguilar, L. Hernández, A. Antillón, D. Macaluso, A. Morales-Mori, O. González-Magaña, D. Hanstrop, A. M. Covington, V. Davis, D. Calabrese, and G. Hinojosa, *J. Quant. Spec. Rad. Trans.* **151**, 217 (2015).
- [36] R. A. Phaneuf, C. C. Havener, G. H. Dunn, and A. Müller, *Rep. Prog. Phys.* **62**, 1143 (1999).
- [37] I. C. Lyons, B. Pert, J. B. West, and K. Dolder, *J. Phys. B: At. Mol. Phys.* **19**, 4137 (1986).
- [38] F. Broetz, R. Trassl, R. W. McCullough, W. Arnold, and E. Salzborn, *Phys. Scr.* **92**, 278 (2001).
- [39] R. Trassl, W. R. Thompson, F. Broetz, M. Pawlowsky, R. W. McCullough, and E. Salzborn, *Phys. Scr.* **80**, 504

- (1999).
- [40] D. Attwood, *Soft X-rays and Extreme Ultraviolet Radiation* (Cambridge University Press, New York, 1999).
- [41] G. C. King, M. Tronc, F. H. Read, and R. C. Bradford, *J. Phys. B: At. Mol. Opt. Phys.* **10**, 3357 (1977).
- [42] S. Ricz, T. Buhr, K. Holste, A. Borovik Jr, D. Bernhardt, S. Schippers, A. Kover, D. Varga, and A. Mller, *Phys. Rev. A*, **81** (2010).
- [43] M. Domke, K. Schulz, G. Remmers, G. Kaindl, and D. Wintgen, *Phys. Rev. A* **53**, 1424 (1996).
- [44] R. D. Cowan, *The Theory of Atomic Structure and Spectra* (University of California Press, Berkeley, California, USA, 1981).
- [45] A. Tauheed and Y. N. Joshi, *Physica Scripta* **80**, 025305 (2009).
- [46] M. J. Seaton, *Rep. Prog. Phys.* **46**, 167 (1983).
- [47] A. Tauheed and Hala, *Phys. Scr.* **85**, 025304 (2012).
- [48] K. G. Dyall, I. P. Grant, C. T. Johnson, and E. P. Plummer, *Comput. Phys. Commun.* **55**, 425 (1989).
- [49] F. Parpia, C. F. Fischer, and I. P. Grant, *Comput. Phys. Commun.* **94**, 249 (2006).
- [50] C. P. Ballance and D. C. Griffin, *J. Phys. B: At. Mol. Opt. Phys.* **39**, 3617 (2006).